

Journal of Biomedical Optics

SPIEDigitalLibrary.org/jbo

Polarization control of Raman spectroscopy optimizes the assessment of bone tissue

Alexander J. Makowski
Chetan A. Patil
Anita Mahadevan-Jansen
Jeffrey S. Nyman

Polarization control of Raman spectroscopy optimizes the assessment of bone tissue

Alexander J. Makowski,^{a,b,c} Chetan A. Patil,^b Anita Mahadevan-Jansen,^{a,b} and Jeffrey S. Nyman^{a,b,c,d}

^aTennessee Valley Healthcare System, Department of Veterans Affairs, Nashville, Tennessee 37212

^bVanderbilt University, Department of Biomedical Engineering, Nashville, Tennessee 37232

^cVanderbilt University, Vanderbilt Center for Bone Biology, Nashville, Tennessee 37232

^dVanderbilt University, Department of Orthopaedic Surgery & Rehabilitation, Nashville, Tennessee 37232

Abstract. There is potential for Raman spectroscopy (RS) to complement tools for bone diagnosis due to its ability to assess compositional and organizational characteristics of both collagen and mineral. To aid this potential, the present study assessed specificity of RS peaks to the composition of bone, a birefringent material, for different degrees of instrument polarization. Specifically, relative changes in peaks were quantified as the incident light rotated relative to the orientation of osteonal and interstitial tissue, acquired from cadaveric femurs. In a highly polarized instrument (10^6 :1 extinction ratio), the most prominent mineral peak (ν 1 Phosphate at 961 cm^{-1}) displayed phase similarity with the Proline peak at 856 cm^{-1} . This sensitivity to relative orientation between bone and light observed in the highly polarized regime persisted for certain sensitive peaks (e.g., Amide I at 1666 cm^{-1}) in unaltered instrumentation (200 :1 extinction ratio). Though Proline intensity changed with bone rotation, the phase of Proline matched that of ν 1 Phosphate. Moreover, when mapping ν 1 Phosphate/Proline across osteonal-interstitial borders, the mineralization difference between the tissue types was evident whether using a 20x or 50x objectives. Thus, the polarization bias inherent in commercial RS systems does not preclude the assessment of bone composition when using phase-matched peaks. © The Authors. Published by SPIE under a Creative Commons Attribution 3.0 Unported License. Distribution or reproduction of this work in whole or in part requires full attribution of the original publication, including its DOI. [DOI: [10.1117/1.JBO.18.5.055005](https://doi.org/10.1117/1.JBO.18.5.055005)]

Keywords: bone quality; polarization; spectrum analysis Raman; composition; structure.

Paper 12677RRR received Oct. 12, 2012; revised manuscript received Apr. 17, 2013; accepted for publication Apr. 19, 2013; published online May 24, 2013.

1 Introduction

Despite recent advances in the ability to assess fracture risk,^{1,2} definitive metrics do not yet exist to identify individuals in need of an intervention that lowers fracture risk. Complementary to established x-ray-based diagnostics of bone, Raman spectroscopy (RS) is an emerging technology that offers nondestructive³⁻⁷ measures of the biochemical nature of tissue. As an indication of its potential to assess fracture risk, RS detected differences in carbonate concentration relative to phosphate between bone samples from nonfracture patients and bones from osteoporotic fracture cases.⁸ In addition to quantifying the amount of carbonate in calcified tissue,⁹ RS is sensitive to local changes in mineral accumulation through mineral to collagen peak ratios, as well as local changes in mineral maturation through measurements of crystallinity.¹⁰ These properties become less heterogeneous with aging,¹¹ change in response to tissue damage,¹² and correlate to mechanical strength of rodent bones,^{13,14} as well as human cortical bone.¹⁰

While these attributes make RS a candidate for clinical diagnosis of bone quality and disease states, unresolved issues regarding instrument polarization and its impact on analysis hamper unambiguous derivation of quantities reflecting the biochemical properties of bone tissue, referred to henceforth as biomarkers. For example, probe-based instruments have been developed to acquire Raman spectra from bone through the

overlying tissue.¹⁵⁻¹⁷ However, most RS studies assessing bone use laser confocal microscopes¹⁸ in which the laser is polarized.^{19,20} Since most fiber optic instruments do not preserve polarization, there is potential for significant discrepancy between the relevant biomarkers of fracture resistance as obtained from RS microscopes and those obtained from existing clinically relevant instruments.

Earlier studies in using Fourier transform infrared spectroscopy (FTIR) identified that vibrational spectroscopy markers for mineralization, crystallinity, carbonation, and collagen cross-linking all significantly associate with fragility fracture,²¹ and while the influence of polarization on FTIR was previously characterized,^{22,23} the polarization state for this instrument was not reported. FTIR and RS are linked as vibrational spectroscopy methods, but fundamental differences give RS an apparent clinical advantage that has fueled cross-correlation and validation in RS.

Recent correlation studies linking RS to the fracture resistance of bone have reported different biomarker sensitivity of RS to the biomechanical properties of bone, possibly due to instrument polarization differences. In one RS study involving a commercial confocal system, differences in ν 1 Phosphate/ CH_2 -wag between trabecular and cortical bone were related to differences in nanomechanical properties between the tissue types.²⁴ In another study analyzing cortical bone from genetic mouse models involving matrix metalloproteinases (Mmp2-/- and Mmp9-/-) and using a similar commercial instrument, correlations among nanoindentation modulus, bending strength, and RS were reported for several mineral-to-collagen ratios, but not ν 1 Phosphate/Amide I.²⁵ On the other hand, strength

Address all correspondence to: Jeffrey S. Nyman, Vanderbilt Orthopaedic Institute, Medical Center East, South Tower, Suite 4200, Nashville, Tennessee 37232. Tel: 615-936-6296; Fax: 615-936-0117; E-mail: jeffry.s.nyman@vanderbilt.edu

of bone from vehicle- and glucocorticoid-treated mice was correlated to various RS peaks when normalized to Amide I in a fiber optic system.²⁶ Despite differences in modes of biomechanical testing among these studies, the polarization state of the instrument likely influences which RS biomarkers are sensitive to experimental groups.

Even though bone is a birefringent material, only a few investigations have intentionally examined the effect of polarization on RS peaks of bone.^{27–30} The vast majority of polarization RS studies of mineralized tissues utilized isolator and analyzer polarizers to “fully polarize” both the input light and collection arm of the Raman system (Table 1). To the best of our knowledge, the extent to which polarization may affect various peak ratios used to assess composition of bone is not well understood for RS instruments without these added optics. Addressing this is important because Raman scattering bands are inherently and differentially affected by polarization due to vibrational modes that give rise to the Raman effect.^{31,32} Even though Legendre polynomials can be used to extract the distribution of collagen and mineral orientation by modulating polarization,³⁰ inherent polarization within the instrument can affect bands even in the absence of molecular organization (e.g., analyzing carbon tetrachloride).³³ Because sample volume, molecular organization, scattering anisotropy, and tissue turbidity influence the scattered light,³⁰ it is difficult to predict how polarization affects RS spectra of bone tissue (which is both turbid and organized), especially when the input laser light is unaltered (Table 1). In the context of RS instrumentation, we refer to changes in Raman peak intensities due to bone rotation (relative to light polarization) as a “polarization bias.”

Rather than intentionally polarizing Raman collection, the present study compares RS biomarkers of human cortical bone with respect to inherent system polarization using commercial instrumentation. The hypothesis of this study was that the intensity of polarization-sensitive Raman bands would oscillate relative to input polarization. Thus, optimization of the relative phase of these Raman bands’ oscillations could yield biomarkers that are better suited for the study of either composition (phase matched and less polarization sensitive) or structure (phase mismatched and polarization sensitive). This study uses polarization theory to quantify the phase and amplitude for a number of Raman peaks of bone, and in doing so, identifies phase matching as the source of polarization insensitivity in known and newly characterized peak ratios of bone composition. Whereas other studies have observed the intensity change of specific peak ratios (Table 1), the present work establishes phase profiles for many of the prominent peaks arising from bone with and without added polarization optics.

2 Methods

2.1 Specimen Preparation

Transverse human cortical bone specimens from the lateral femur midshaft were prepared as per previously published methods.¹⁸ Briefly, bone samples were mounted to slides using cyanoacrylate and ground on silicon carbide papers of sequential grit, then polished with 0.05 μm alumina beads in solution to an ultimate surface area of $\sim 8 \times \sim 8 \text{ mm}^2$ and thickness of approximately 4 mm. One sample from each of 6 donors was used (4 males ages 48, 80, 82, and 94 and 2 females ages 86 and 95). To generate a control sample, a human molar was embedded in polymethylmethacrylate; a thick section was cut

in the longitudinal direction; and the surface polished as previously described.¹⁸

2.2 Raman Instrumentation

To fully examine the influence of instrument polarization and bone structure on collected Raman spectra, we conducted several experiments, each with a different collection protocol or degree of polarization. Raman spectra were acquired from the polished surface of the bone tissue in air using a standard confocal Raman microscope (Ramanscope Mark III and InVia Raman Microscope, Renishaw, Hoffman Estates, Illinois) equipped with Renishaw EasyConfocal, a 35 μm slit opening, and a spectral resolution of 1 cm^{-1} , equipped with a 785 nm laser diode source with a polarization extinction ratio (PER) of 200:1 (Innovative Photonic Solutions, Monmouth Junction, New Jersey). To eliminate grating bias according to Renishaw specifications, the polarization was aligned upright within the instrument (left-right when operator faces stage), confirmed with known polarizers and silicon standard intensity. Placing a mirror in the sample plane, the PER was also measured as 20:1 after the dichroic and 17:1 after the grating. Additional optics increased polarization of the Raman microscope, such that the system operated in a highly polarized regime. An isolator (NIR linear polarizer, 1000:1 extinction ratio, Thorlabs, Newton, New Jersey) was used to isolate a polarization angle of input laser light prior to sample incidence. An analyzer (additional linear polarizer, same specifications) isolates a particular polarization angle of light reflected off the sample. A quartz wedge depolarizer (AR coated achromatic depolarizer DPU-25-B, Thorlabs, Newton, New Jersey) effectively scrambles the polarization state of light in space prior to the spectral grating to prevent instrumentation bias by transmitting a pseudo-random polarized beam. Removal of the analyzer (1000:1 extinction ratio) decreased system polarization sensitivity, but retaining the input polarizer provided an “input polarization regime.” In this regime, the bone sample is rotated to examine bias and the depolarizer remains in the system to minimize instrumentation bias of the grating. Without added optics, the system retains a degree of inherent polarization sensitivity, henceforth referred to as an “unaltered polarization regime.”

To preserve system throughput across experiments despite differences in added optics, spectral acquisition exposure times were scaled to ensure 480 mW·s apparent exposure at the sample. This provided a signal to noise ratio (SNR) for the low intensity Proline peak in excess of 10:1 in highly polarized experiments, translating to at least 25:1 in unaltered experiments. Unless otherwise stated, spectra were obtained with 3 accumulations after 5 s photobleaching. Spectra were then binned to a resolution of 3 cm^{-1} , and processed via least squares modified polynomial fit³⁹ and smoothed for noise using a 2nd order Savitsky-Golay filter.^{26,40} After fluorescence subtraction, a linear baseline subtraction (based on derivative zero-crossings neighboring the peak) was conducted on peaks that overlap with other constituents to ensure no residual fluorescence, namely Proline, Hydroxyproline, $\nu 1$ Phosphate, and Carbonate. Spatial resolution for each objective used was approximated via edge detection on a polished silicon standard. System Raman shift calibration was accomplished using a neon lamp and a silicon standard with Renishaw software to account for grating motion. Silicon measurements before and after each beam path change and

Table 1 Previous polarized Raman studies used altered instrumentation to analyze mineralized tissues and collagen.

Tissue	Instrumentation	Polarization	Laser (nm)	Factor(s)	Raman property	Reported trends	Ref.
Human tooth enamel	Spectrophotometer coupled to microscope with 100x and 50x objectives	Fully polarized ^a	632.8, 514	Crystalline orientation	$\nu_1\text{PO}_4$, $\nu_2\text{PO}_4$, $\nu_3\text{PO}_4$, $\nu_4\text{PO}_4$, $\nu_1\text{CO}_3$, OH	Carbonate preserves the orientation of enamel crystals. Vibrational modes of enamel rods are reconciled to theory.	34
Human tooth enamel	Confocal microscope, 10x objective	Fully polarized	830	Caries and lesions	$\nu_1\text{PO}_4$	Depolarization ratio and anisotropy of $\nu_1\text{PO}_4$ changes between sound enamel and caries. Depolarization ratio and anisotropy of $\nu_1\text{PO}_4$ changes between sound enamel and caries.	35
Sheep tendon, fixed human femur	Confocal microscope, 100x objective NA = 0.8	Not reported	633	Collagen Fiber distribution along osteon radius, and bone rotation	$\nu_3\text{PO}_4/\nu_1\text{PO}_4$, Amide I/Amide III, and Amide III ratio (1271/1243)	Polarization-sensitive peak ratios varied with distance from haversian canal.	29
Rat tail tendon collagen fibrils	Confocal microscope, 60x NA = 1.0 objective	Fully polarized	785	Mechanical stress	Amide I, Amide III	Stress changes orientation distribution but not vibration frequencies of collagen.	36
Whole and powdered mouse tibia	Custom confocal Raman microprobe, various objectives	Fully polarized	785	Osteogenesis Imperfecta (oim)	$\nu_1\text{PO}_4$, Amide I	Orientation distribution of mineral and collagen differ in oim mice.	30
Collagen from bovine achilles tendon	Confocal microscope 60x objective NA = 0.75	Collection arm polarized	633	Collagen fiber orientation	Amide I, Amide III, and Amide III ratio (1245/1268)	Amide III doublet is sensitive to orientation.	33
Turkey leg tendon, embedded mouse femurs	Confocal microscope, 60x NA = 1.0, 20x NA = 0.4	Fully polarized	785	Orientation of cut, depolarization	$\nu_1\text{PO}_4$ /Amide I, $\nu_2\text{PO}_4$ /Amide III, Carbonate/ $\nu_2\text{PO}_4$	Tissue age affects Raman polarization. Collagen orientation obtained from polarized mapping.	19
Embedded human femur osteons	Confocal microscope, 100x NA = 0.9	Not reported	532	Tissue type and orientation	$\nu_1\text{PO}_4$ /Amide I, $\nu_2\text{PO}_4$ /Amide III, $\nu_4\text{PO}_4$ /Amide III	Tissue types have differential polarization sensitivity.	28:37
Femoral head spongy bone	Confocal microscope, 50x objective NA = 0.5	Fully polarized	785	Specimens from osteoporotic fracture patients.	$\nu_1\text{PO}_4$ /Amide I, $\nu_2\text{PO}_4$ /Amide III, $\nu_4\text{PO}_4$ /Amide III, Carbonate/ $\nu_2\text{PO}_4$	Polarized Raman helps determine the location of collagen fibers within trabeculae.	38
Human femur	Confocal microscope, 50x objective NA = 0.75, 20x objective NA = 0.4	Inherent polarization	785	Tissue type and orientation	Various	Polarization sensitivity inherent in peaks and Raman instrumentation can be minimized by optimizing peak phase.	Current Study

^aFully polarized indicates the use of polarizing optics in the input and collection arm.

at system “startup” ensured wavenumber calibration consistency.

Since dentin has less heterogeneity in collagen fibril orientation than bone, we collected Raman spectra from the same site as a human tooth rotated from 0 deg to 180 deg in 20 deg increments in order to characterize the polarization sensitivity of our RS instrument without additional polarization optics. In these dentin measurements, known polarization sensitive peaks oscillated through rotation with percent changes in mean normalized intensity of 6.6% and 22.6% for ν_1 Phosphate and Amide I, respectively.

2.3 Experimental Design

2.3.1 Highly polarized analyzer rotation

Polarization analysis used known bias from previous work^{19,28,37} to confirm the ability of Malus’s law to model phase and amplitude of Raman peaks. In effect, our first experiment was designed to evaluate phase oscillation for sensitive RS peaks. To account for within sample variation, five osteons and neighboring interstitial sites were selected from a single bone sample.¹⁸ In brief, selected osteons were spaced evenly over the surface and distributed by osteon size and pore size. Using upright input polarization through our 50 \times , numerical aperture (NA) = 0.75 objective (lateral resolution 3 to 4 μm , as measured by edge detection) and stationary bone orientation, the analyzer was rotated at each site from 0 deg to 180 deg in 20 deg increments. This study used an adaptation of Porto’s notations based on microscope translation stage directions since Porto’s notations traditionally depend on sample crystallographic axis,^{41,42} which varies within cortical bone. In this adaptation, the polarization regime is Z(XB)-Z, where B denotes analyzer rotation relative to instrument input X (always left-to-right as viewed by operator). Intensity for each of the prominent peaks in the bone spectrum was then modeled as a function of polarization angle B to compare the degree of oscillation between quantities.

2.3.2 Bone rotation for two polarization regimes

Next, spectra were collected as a function of bone orientation to evaluate peak and peak ratio sensitivity in less polarization sensitive systems. We analyzed a single osteon and neighboring interstitial site from each of three bones under both input polarized (added isolator and depolarizer) or unaltered (no added optics) polarization regimes. As was done with tooth, the bone sample was rotated around the optical axis using a custom stage to preserve collection location while obtaining spectra (50 \times , NA = 0.75 objective) from 0 deg to 180 deg rotation in 20 deg increments. The polarization regime is Z(X x)-Z, where x denotes bone rotation around Z relative to instrument input X (left-to-right as viewed by operator).

2.3.3 Spectral mapping of bone tissue rotation

Using the unaltered polarization regime, we acquired confocal Raman maps of spatial heterogeneity to demonstrate the effects of phase-matching on compositional discrimination of known osteonal and interstitial tissue differences. Phase-matching of peak ratios is defined as minimizing the phase difference of the ratio components, effectively choosing peaks that have the most similar rotation angle of maximum intensity, subsequently reducing the impact of rotation angle

upon the observed ratio intensity. One osteon and the neighboring interstitial area (20 \times , NA = 0.4 objective, lateral resolution of 12 μm) from each of three bones was mapped using unaltered instrumentation at a pixel size of 8 \times 8 μm for 0 deg, 45 deg, and 90 deg rotations of the bone sample about the optical axis. To analyze discrimination of osteonal from interstitial tissue, intensity maps were generated for selected peak ratios applying a uniform scale based upon full intensity range, such that a polarization insensitive spectral constituent will show the same intensity image in all three acquisitions. Instrument polarization in direction X is denoted with X-Y stage directions in each figure panel. For one bone, the mapping process was repeated using the 50 \times objective for an osteonal-interstitial border within the original 20 \times map to demonstrate Raman maps of polarization bias with a smaller sample volume.

2.4 Data Modeling and Statistics

Data modeling and statistics were performed on peak heights extracted from each processed spectrum [Fig. 1(a)]. Peak intensities were modeled to Malus’ Law^{43,44} (intensity varies with polarization angle as a function of cosine squared) for phase and amplitude of oscillation [Fig. 1(b)]. The custom algorithm employed a least squares fit for amplitude nested inside a mean squared error driven optimization (Matlab implementation of Nelder-Mead simplex,⁴⁵ Mathworks, Natick, Massachusetts), outputting peak phase, amplitude, and mean intensity as illustrated in Fig. 1(b). The degree of orientation sensitivity across the three generated polarization regimes was quantified for each prominent peak as a function of oscillation amplitude normalized to mean peak intensity. For less sensitive peaks, individual sample oscillations could become noisy or undetectable, such that data fails the underlying assumptions of the Malus’ law model. Modeled data were excluded from quantitative analysis if the model fit was not significant ($p < 0.05$) via analysis of variance (ANOVA) regression (all fits shown in figures and tables are significant). For each peak, the number of samples with statistically significant models and the observable percent change in intensity measurements of the same quantity were recorded.

3 Results

3.1 Phase Differences in Raman Peaks of Bone Under Highly Polarized Light

Acquired under a highly polarized regime, RS biomarker peaks exhibited differential polarization behavior in both degree and relative phase of intensity oscillation. For the most part, relative phase varied insignificantly between osteonal and interstitial tissue types for any given peak. However, phase oscillation varied distinctly between different peaks representing the same bone compositional element (i.e., Amide I at 1666 cm^{-1} versus Amide III at 1247 cm^{-1} , both biomarkers of collagen in Fig. 2). In reference to the ν_1 Phosphate peak (961 cm^{-1}), the strongest spectral signal for bone mineral, Proline (854 cm^{-1}) was found to have the best phase match for the generation of a mineral to collagen ratio, a metric commonly used as an indicator of bone quality.

Building upon our previous findings,¹⁸ the observed difference between osteonal and interstitial tissue composition (Fig. 3) was small (2% to 30% difference) relative to intensity change as a function of polarization angle (100% to 300%

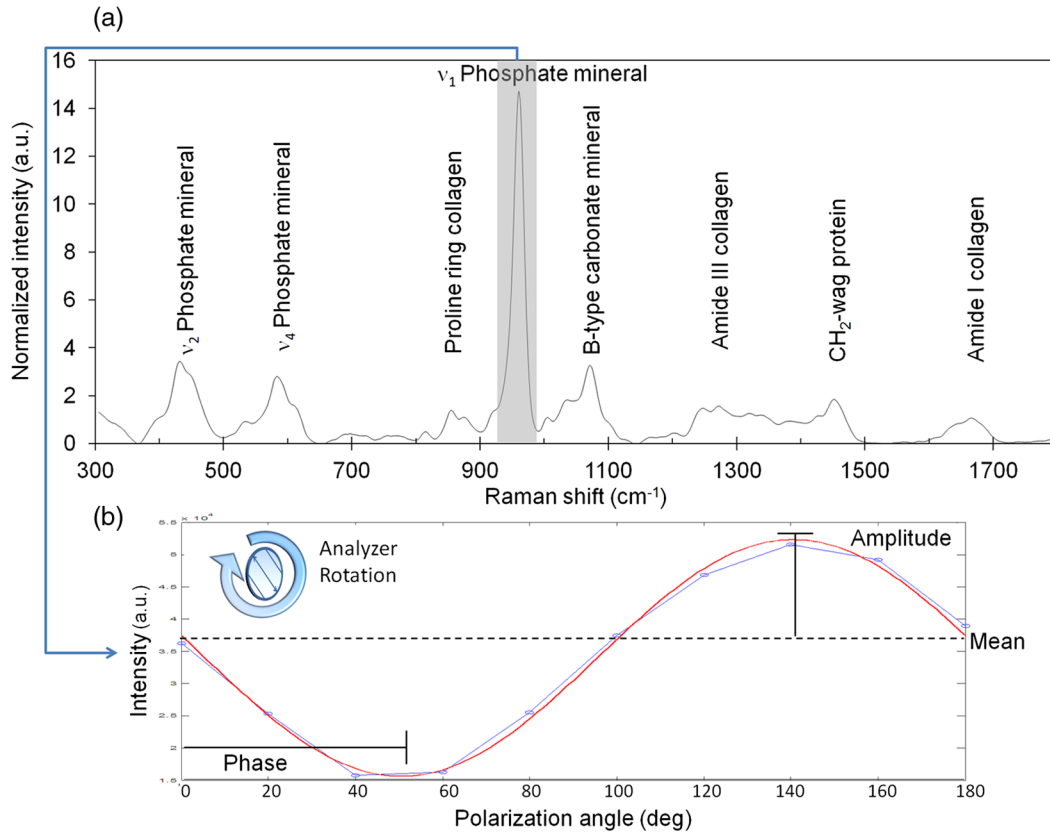


Fig. 1 Diagram of representative labeled Raman spectrum of bone shows feature extraction. (a) ν_1 Phosphate peak intensity is extracted from a wave-number range and baselined. (b) Actual data from highly polarized osteon analysis shows ν_1 Phosphate intensity for each analyzer rotation (output polarization angle). Data is then modeled to a sinusoidal fit to extract phase, amplitude, and mean intensity. Shown here for analyzer rotation, this method was also used in bone rotation experiments.

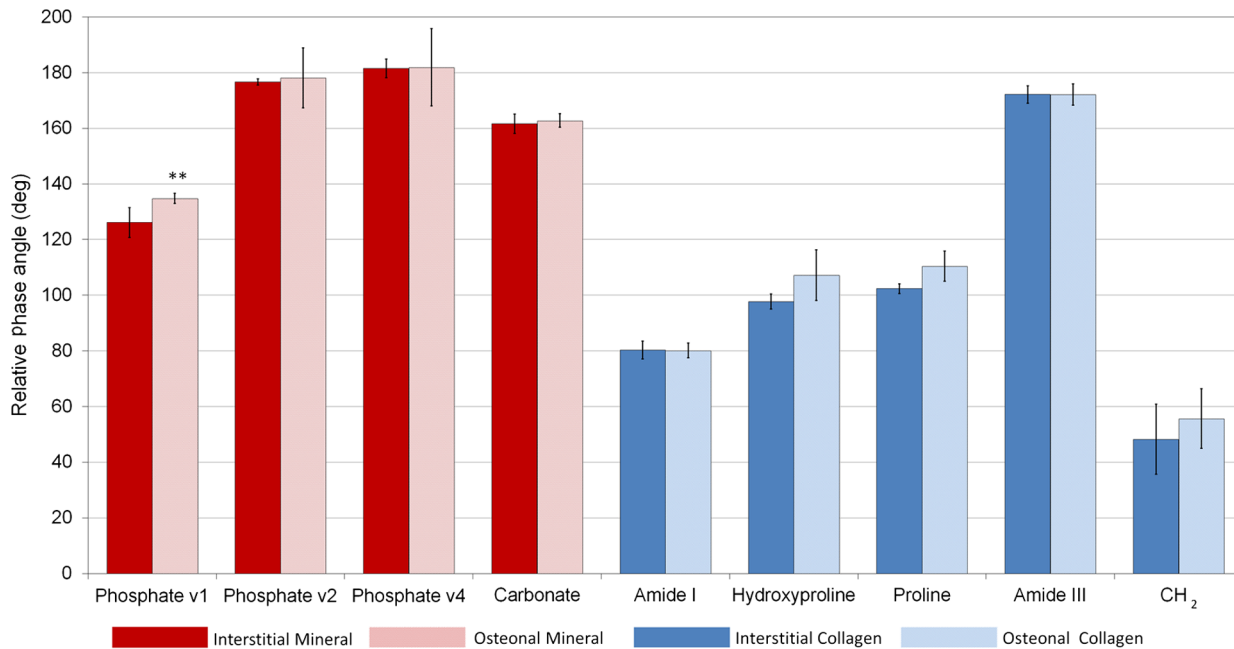


Fig. 2 Relative phase angle (mean \pm SD) from highly polarized analysis of osteons, conducted with analyzer rotation, shows few differences between tissue type but strong compositional element differences in phase angle. The phase range of ν_1 Phosphate was closest to the phase range of Proline and CH₂-wag. In this regime, Amide I is the collagen peak with the greatest phase difference from ν_1 Phosphate. ** Only ν_1 Phosphate had a significant difference $p < 0.05$ in phase between osteonal and interstitial tissue types by two-sided Student's *t*-test.

difference). However, under the traditional calculation of a mineral to collagen ratio using $\nu 1$ Phosphate (mineral) and Amide I (collagen) as biomarkers, different quantities would be observed at different polarization angles [e.g., 60 deg versus 140 deg in Fig. 3(a)]. As an alternative mineral to collagen ratio that still utilizes the signal strength of $\nu 1$ Phosphate, the phase-matched Proline peak can be used to represent collagen [Fig. 3(b)]. Also, as indicated by Kazanci et al.,²⁸ other RS mineral quantities can be substituted for $\nu 1$ Phosphate [Fig. 3(c) and 3(d)]. The distinct phase mismatch between $\nu 2$ Phosphate and Amide I [Fig. 3(c)] was reversed by using Amide III for collagen [Fig. 3(d)].

3.2 Susceptibility of Certain Raman Peaks to Polarization Bias

When defined as the model amplitude normalized to mean peak intensity, the peak sensitivity to polarization decreased from the highly polarized regime to the input polarized and unaltered polarized regimes (Fig. 4). Hydroxyproline (870 cm^{-1}) and Amide I, the two most sensitive in the highly polarized regime, remained polarization sensitive in the input polarized regime. Despite the fact that spectra were acquired from different bone samples, the oscillation sensitivity trends among most peaks remain consistent between the highly polarized and input polarized regimes. Comparing input polarized and unaltered

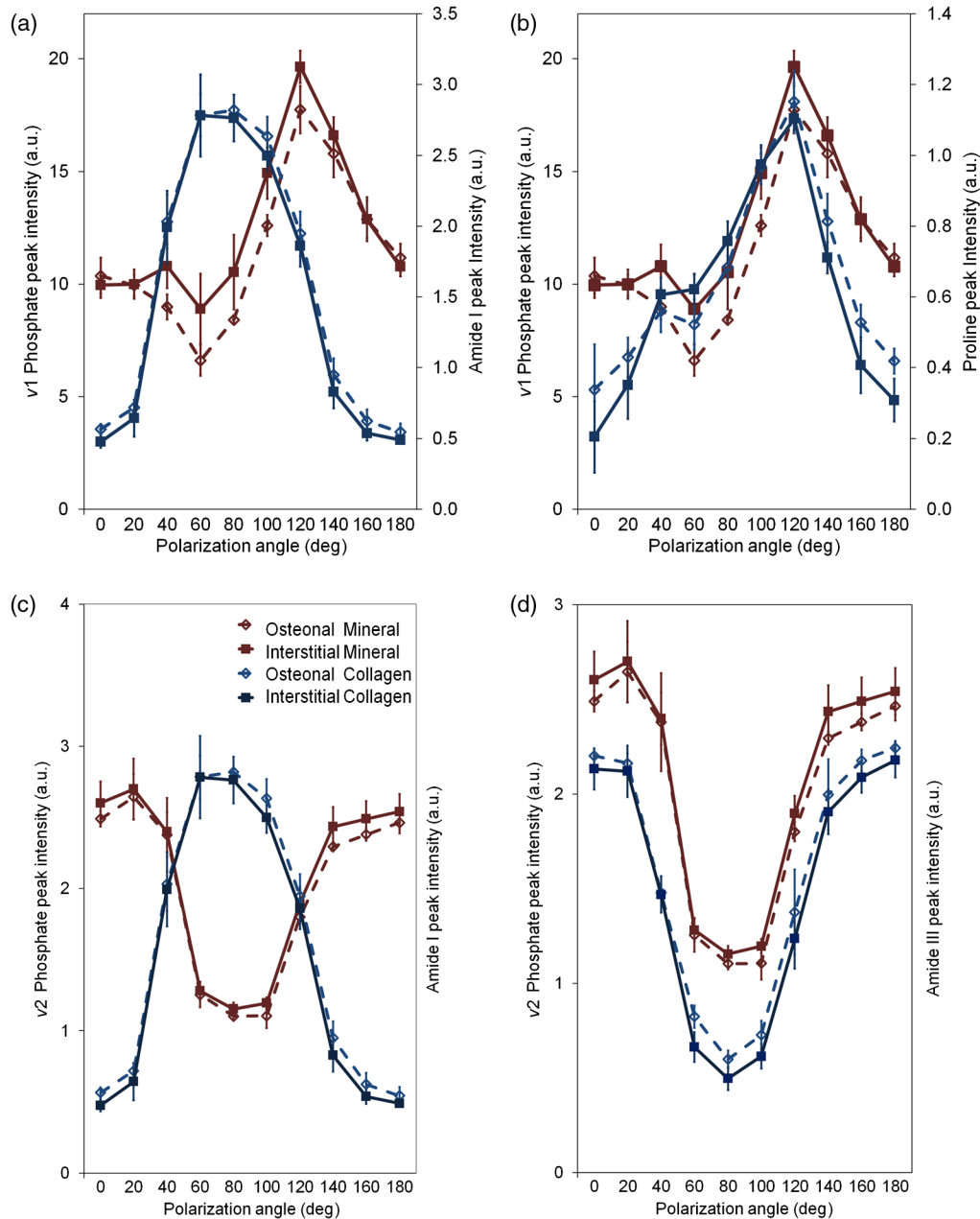


Fig. 3 Phase mismatch of peak intensity versus polarization angle [$\nu 1$ Phosphate and Amide I, (a)] leads to polarization bias of mineral to collagen ratio that can be eliminated by using Proline to represent collagen (b). Alternative biomarkers of mineral to collagen ratio can also be phase matched [$\nu 2$ Phosphate and Amide III, (d)] to eliminate Amide I polarization bias (c). This phase matching prevents spurious conclusions about osteonal and interstitial differences due to polarization angle.

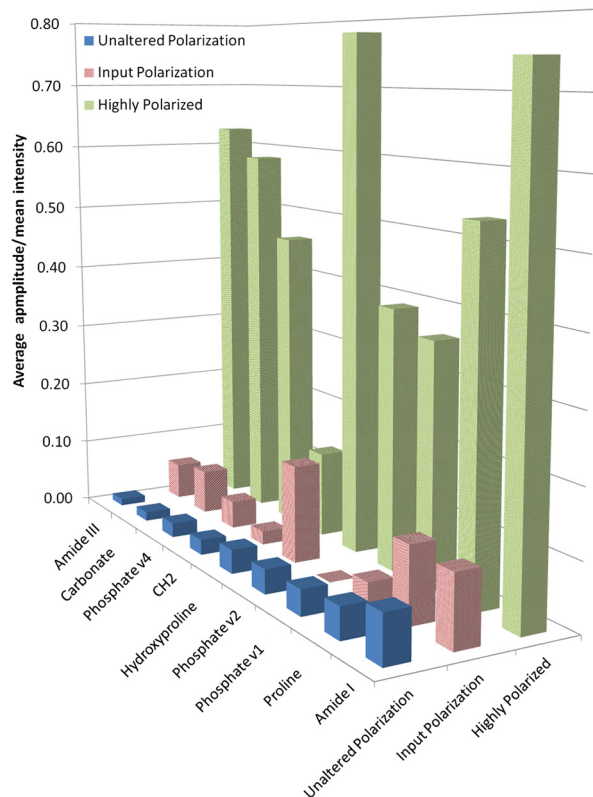


Fig. 4 Average model amplitude normalized to mean intensity shows a preservation of peak oscillation trends with decreasing polarization. Highly polarized data (green) shows greater sensitivity than input polarized data (red). Less sensitive peaks like Amide III continue to drop in sensitivity in the unaltered polarization regime (blue), whereas more sensitive peaks like Amide I show consistent sensitivity.

polarization regimes (paired measurements of the same sample locations at the same rotation increments), polarization sensitivity dropped off markedly for some peaks like Carbonate and Hydroxyproline (Fig. 4). However, for other peaks like Amide I and ν_1 Phosphate, degree of oscillation amplitude remains relatively unchanged. In the unaltered polarization regime, less sensitive peaks like Amide III fell into the noise floor, as evidenced by decrease in number of significant model fits by ANOVA regression (Table 2).

An RS surface plot for a single osteon acquired with unaltered polarization [Fig. 5(a)] illustrates that ν_1 Phosphate peak intensity fluctuations [Fig. 5(b)] were out of phase with Amide I intensity fluctuations [Fig. 5(c)] but matched to the fluctuations of Proline [Fig. 5(d)]. Although noise has a significant impact on model fit in the unaltered regime, the trends of polarization phase between mineral and collagen peaks (Fig. 5) remained consistent with trends observed when the analyzer was rotated with the bone sample stationary (Fig. 3). Phase mismatch trends of RS biomarkers from highly polarized data persisted in unaltered polarization.

3.3 Performance of Phase-Matched Ratios for Compositional Differences

RS maps demonstrate how phase mismatch in RS peak ratios confounds the consistent measurement of spatial heterogeneity, even in an unaltered polarization regime (Fig. 6). Expected differences in mineral to collagen ratio between an osteon and surrounding interstitial tissue is not maintained throughout bone rotation for polarization sensitive ν_1 Phosphate/Amide I [Fig. 6(b)]; whereas, ν_2 Phosphate/Amide III [Fig. 6(c)] shows consistent overall intensity differences between the tissue types despite rotation. Yet, this latter image is noisier than the

Table 2 Peak sensitivity ranking as a percent change in intensity during bone rotation shows that some peaks still oscillate with unaltered system polarization.

Raman peak ^a	Highly polarized ^a		Input polarized		Unaltered polarization	
	% Change ^c	Sig. models ^d	% Change	Sig. models	% Change	Sig. models
Amide III	125.2	9/10	11.2	4/6	2.2	1/6
Carbonate	116.5	10/10	13.5	5/6	2.8	1/6
ν_4 Phosphate	91.7	9/10	8.4	1/6	4.4	2/6
CH ₂	26.0	10/10	4.1	2/6	4.6	1/6
Hydroxyproline	156.0	8/10	29.4	5/6	7.3	1/6
ν_2 Phosphate	77.9	8/10	N/A ^e	0/6	7.4	2/6
ν_1 Phosphate	71.9	10/10	6.2	5/6	7.8	3/6
Proline	106.7	8/10	22.7	5/6	9.5	4/6
Amide I	149.1	10/10	21.2	6/6	14.4	5/6

^aDerived from separate samples.

^bRank is based on the degree of mean normalized intensity fluctuation for unaltered polarization.

^c% Change is defined as the range of observed intensities normalized to the mean intensity observed during specimen rotation (unaltered and input polarized) or during analyzer rotation (highly polarized) for significant (sig.) model fits. When more than one model fit is significant, the mean is given.

^dNumber of significant models. Significance of model fit is defined as $p < 0.05$ of the ANOVA regression (goodness of fit).

^eN/A: No significant models.

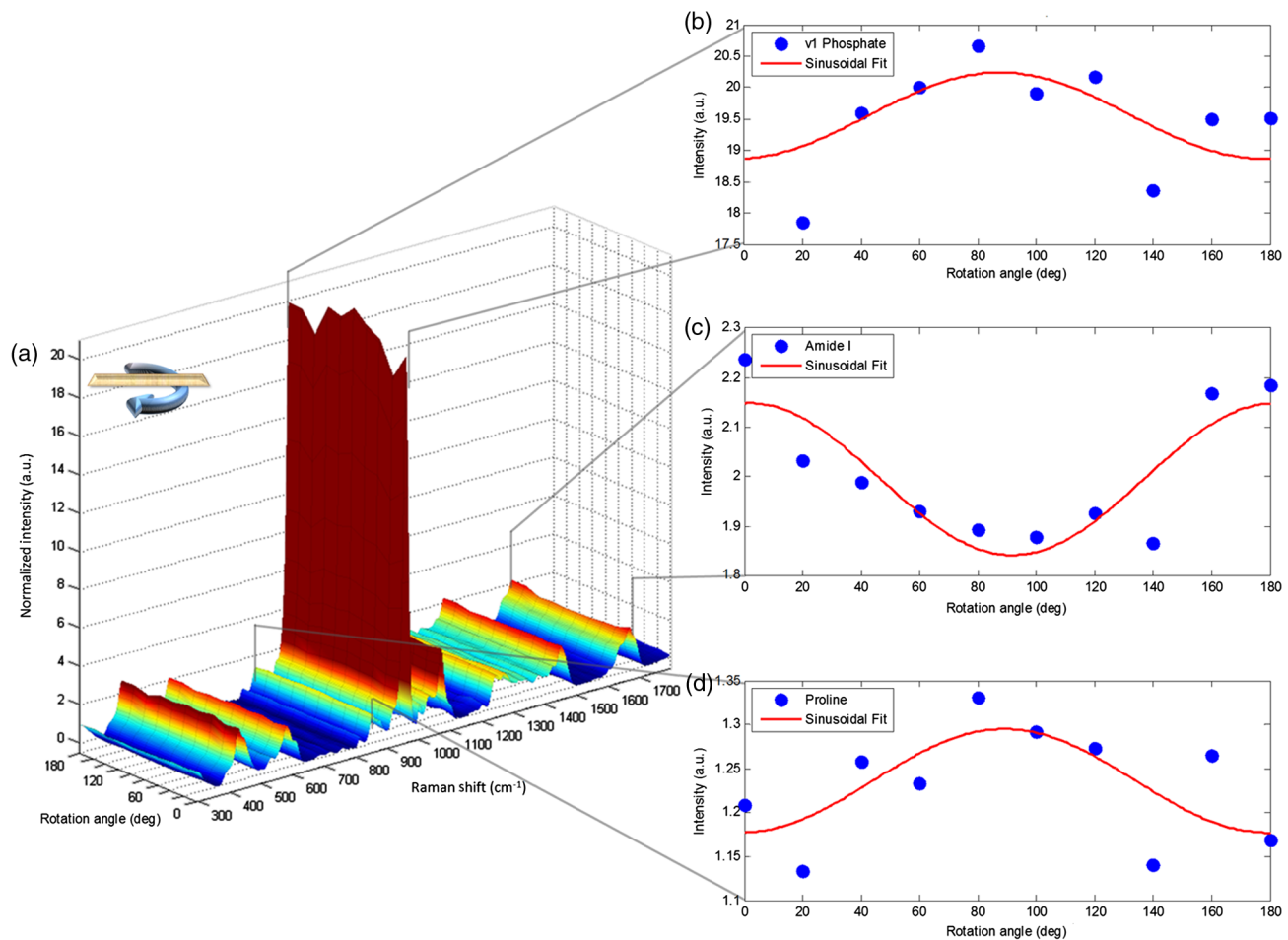


Fig. 5 Surface plot of osteonal sample bone rotation under unaltered polarization setup indicates persistence of phase mismatch for mineral to collagen components. (a) Intensity colored surface plot shows spectral variance due to rotation angle. Cutaways show $\nu 1$ Phosphate peak intensity (b) is out of phase with Amide I (c) while in phase with Proline (d).

former image due to significantly lower SNR of the $\nu 2$ Phosphate and Amide III peaks, relative to $\nu 1$ Phosphate. Maps of $\nu 1$ Phosphate/Proline [Fig. 6(d)] illustrate a relatively consistent image of compositional heterogeneity throughout rotation, differentiating the osteonal tissue from the more mineralized interstitial tissue. This peak ratio map is independent of bone rotation because of the low phase difference between $\nu 1$ Phosphate and Proline (Table 3).

Figure 7 shows how NA and subsequent differences in sample volume averaging affect the apparent sensitivity of mineral to matrix calculations to tissue type. The calculations compare $\nu 1$ Phosphate/Amide I sensitivity to the phase-matched $\nu 1$ Phosphate/Proline using a map at 20 \times magnification and a 50 \times map of a portion of the same area [Fig. 7(a)]. The polarization sensitive Amide I ratio produced a distinct intensity change at 50 \times magnification in the 45 deg map [Fig. 7(c)] that was less pronounced but arguably still apparent at 20 \times [Fig. 7(b)]. The mineral to matrix ratio with Proline [Fig. 7(d) and 7(e)] was relatively consistent throughout.

4 Discussion

Development of RS methods towards bone diagnostics requires a firm understanding of which RS measures are sensitive to bone tissue composition and which are sensitive to bone tissue

organization. While the potential for highly polarized RS to discriminate bone organization is known (Table 1), the present study provides a thorough characterization of the contribution of polarization bias in a standard Raman microscope to RS measurements of bone. When the goal of RS analysis is to assess compositional differences in bone, polarization bias adds uncertainty to the measurements. The addition of polarization optics, even to reduce polarization bias, leads to increased data collection time. Therefore, this study characterized peak and peak ratio specificity without altering instrumentation and found that polarization bias exists in a standard microscope and needs to be addressed.

Consistent with findings from the highly polarized RS analysis of mouse bone by Raghavan et al.,³⁰ polarization bias can persist for a low NA objective (NA = 0.4) (Fig. 7) that effectively averages the signal over larger spatial volumes than a 50 \times objective with a NA of 0.75. Nonetheless, matching polarization-orientation phase, effectively matching the organizational component of RS peaks, allows for consistent measures of composition [Fig. 3(b) and 3(d), as well as Fig. 7(c) and 7(d)]. This study used spectral maps of spatial heterogeneity within bone (Fig. 6) to establish that peak ratio sensitivity identified by polarized RS studies (Table 1) remains in unaltered polarization regimes (i.e., standard confocal RS instruments). In effect, polarization phase can be exploited to distinguish compositional

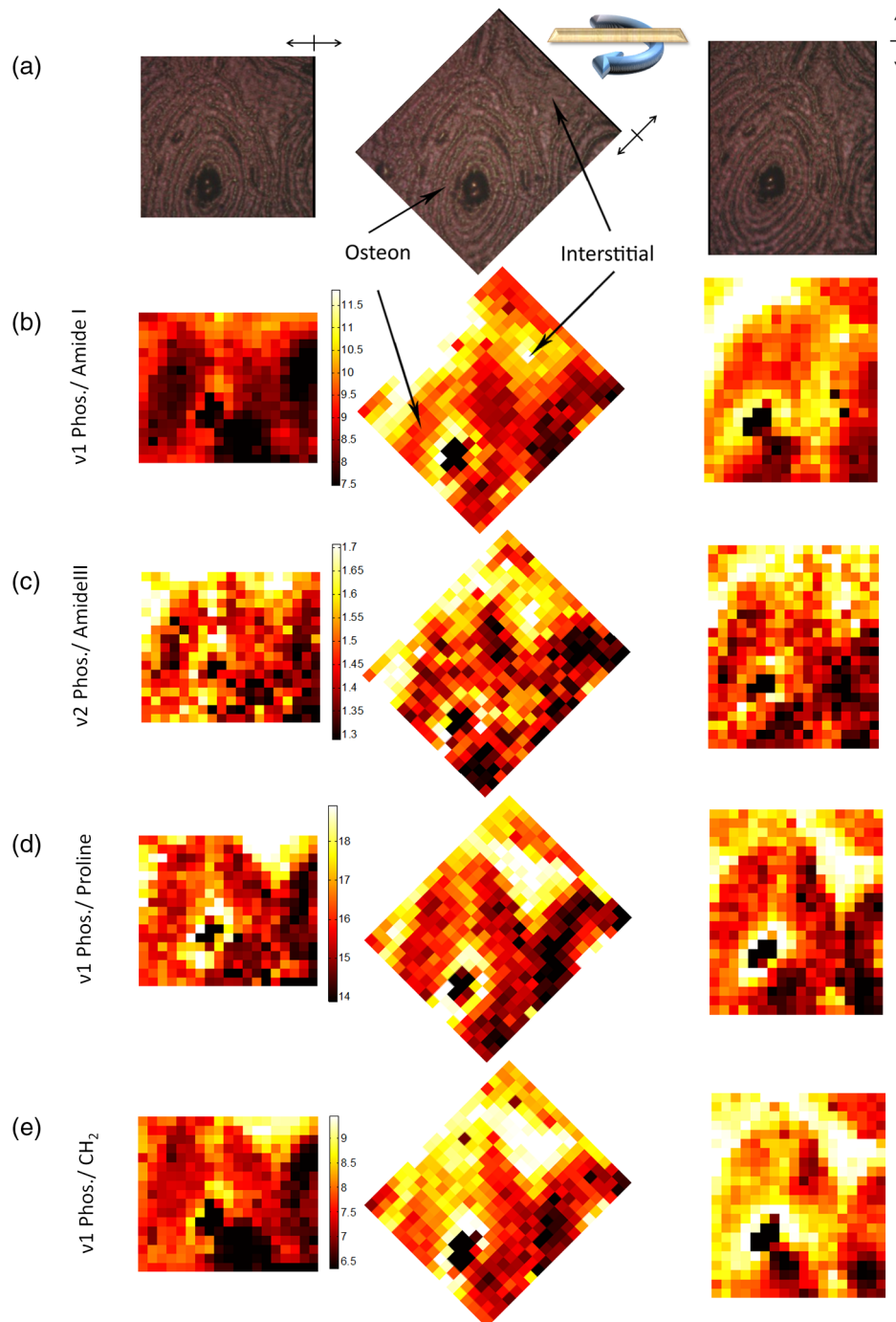


Fig. 6 Mineral to collagen biomarker heat maps of derived peak ratios validate differential rotational consistency. (a) Bright field images reference the rotation of the osteon in 45 deg increments from left to right. Color maps are set to universal scale within each quantity and frames are rotated so that same image should be apparent under a lack of polarization sensitivity. (b) ν_1 Phosphate/Amide I shows greatest rotational dependence. (c) ν_2 Phosphate/Amide III consistency is masked by noise due to lower peak intensities. (d) ν_1 Phosphate/Proline shows rotational consistency with a lower noise floor. (e) ν_2 Phosphate/ CH_2 shows strong rotational dependence.

heterogeneity from organizational heterogeneity. Finally, throughput costs of added optics can be avoided by using less sensitive peaks and phase-optimized peak ratios.

Spectral fingerprints of disease may rely upon organization of collagen and mineral as much as the relative composition of these constituents. This is of particular importance because bone disorders and disease states including osteoporosis and osteogenesis imperfecta can involve deleterious changes in bone

organization.³⁰ Moreover, the organization of the constituents of bone tissue influences the fracture resistance of bone.^{46–50} The observations of phase difference (Fig. 2) from our modeling of spectral data as a function of analyzer rotation is consistent with findings from previous highly polarized studies,^{19,28,37} as well as recent theoretical models of collagen orientation within osteons.⁵¹ The phase differences between RS biomarker peaks arise from the organization of mineral crystals and collagen

Table 3 Paired phase difference between selected Raman peak ratios and overall variance of peak ratios were estimated for bone and tooth rotation using the unaltered polarization instrument.

Peak ratio	Representation	Bone samples		Dentin control	
		Phase difference (deg) ^a	Coefficient of variation ^b	Phase difference (deg)	Coefficient of variation
ν 1 Phosphate/Amide I	mineral:collagen	69.9	0.073	85.5	0.110
ν 2 Phosphate/Amide III	mineral:collagen	N/A ^c	0.0004	0.1	0.021
ν 1 Phosphate/Proline	mineral:collagen	2.2	0.023	9.2	0.040
ν 1 Phosphate/CH ₂	mineral: protein	62.8	0.038	85.2	0.054
Carbonate/ ν 1 Phosphate	carbonate substitution	0.1	0.020	3.1	0.009
Carbonate/ ν 2 Phosphate	carbonate substitution	N/A ^c	0.025	6.5	0.016
Carbonate/ ν 4 Phosphate	carbonate substitution	31.6	0.022	9.3	0.022

^aTo obtain phase difference, the difference in phase between paired peaks (same spectra for the same site of rotation) was averaged among the multiple sites of data collection in which model fit was significant for both peaks.

^bTo obtain coefficient of variation, the standard deviation per mean of the peak ratio for a given rotation was averaged across multiple sites of data collection.

^cN/A: No phase angle could be generated from significant models within the same sample. Significance of model fit is defined as $p < 0.05$ of the ANOVA regression (goodness of fit).

fibrils, such that information encoded within polarization phase may provide new insight for future disease diagnosis or fracture risk assessments. However, clear associations of phase and bone's fracture resistance remain to be established. Nonetheless, as RS matures toward clinical use, consistency in discriminating composition from organization may contribute to accurate assessment of fracture risk.

Alternatively, RS could prove especially effective in the diagnosis of bone diseases that are pathologically based upon bone composition, including diabetes, chronic kidney disease, and the discrimination of grades of osteogenesis imperfecta. Recent investigations employing spatial sampling regimens to average out polarization bias concur that alternative mineral to collagen ratios (Fig. 6) exhibit increased sensitivity to known osteonal and interstitial differences in composition.^{18,52} Specifically, improvement in mineral to collagen ratio variance and microstructure delineation when utilizing Proline instead of Amide I as a collagen component can be explained by a decrease in underlying polarization phase difference between ν 1 Phosphate (mineral constituent) and Proline (collagen constituent) (Table 3).

RS acquisition of bone spectra often spans a range of 300 to 1800 cm^{-1} to cover prominent peaks, though it is expanded in some studies to 3000 cm^{-1} to capture a CH peak. Collecting Proline, ν 1 Phosphate, and Carbonate would require spanning only 300 cm^{-1} , further reducing necessary instrumentation, data processing, and collection time. Despite the availability of commercial systems, RS instrumentation differs largely between research groups and studies, implying that polarization bias from orientation sensitive peaks may vary between studies.

Changes in Raman spectra as the bone or tooth rotates relative to the incident laser light reveal the persistence of a polarization-orientation bias for sensitive peaks like Amide I even within less sensitive unaltered RS setups. Polarization sensitivity trends (Fig. 4) are conserved among prominent peaks in both the highly polarized regime and in the input polarized regime,

despite the fact that spectra were acquired from different bone samples. Phase trends seen in highly polarized acquisition of bone appear to persist in unaltered instrumentation as well (Fig. 5). Phase-matched peak ratios of mineral to collagen ratio demonstrate lower coefficients of variation and therefore greater consistency (Table 3). When determined from the same site of bone rotation and then averaged across the various sites, the phase difference between ν 1 Phosphate and Proline was 2.2 deg for bone and 9 deg for more highly organized dentin (Table 3), suggesting that these trends in phase difference may be conserved between tissues and anatomical locations. Despite the low intensity of Proline, the high intensity of the ν 1 Phosphate peak may make ν 1 Phosphate/Proline a more practical compositional metric than ν 2 Phosphate/Amide III, which also has a low paired phase difference (Table 3). In addition, the use of peak phase difference confirmed the compositional nature of carbonate substitution (Table 3). While results suggest optimal metrics for bone composition and caution against possible inconsistent use of other metrics, the polarization-orientation information of RS biomarkers may have greater implications for future clinical bone diagnostics.

Consistent use of less polarization sensitive peaks or phase-matched ratios may allow for clearer comparisons between instruments and studies. RS sensitivity to glucocorticoid-treatment in rheumatoid arthritis bone shows compositional difference despite normalization to Amide I when using a fiber optic (polarization insensitive) system.²⁶ These biomechanical correlations are likely separate and distinct from RS correlations to collagen tension changes seen in formal polarization analysis.³⁶ Given low instrument polarization and results from less polarization sensitive carbonate and Amide III bands, analysis of bone from osteoarthritic patients on different load bearing surfaces can be interpreted as a largely compositional effect.⁵³ Phase mismatch of ν 1 Phosphate/CH₂ [see Figs. 2 and 6(e)] may have contributed to biomechanical correlation due to use of a commercial confocal system,²⁴ thereby indicating a

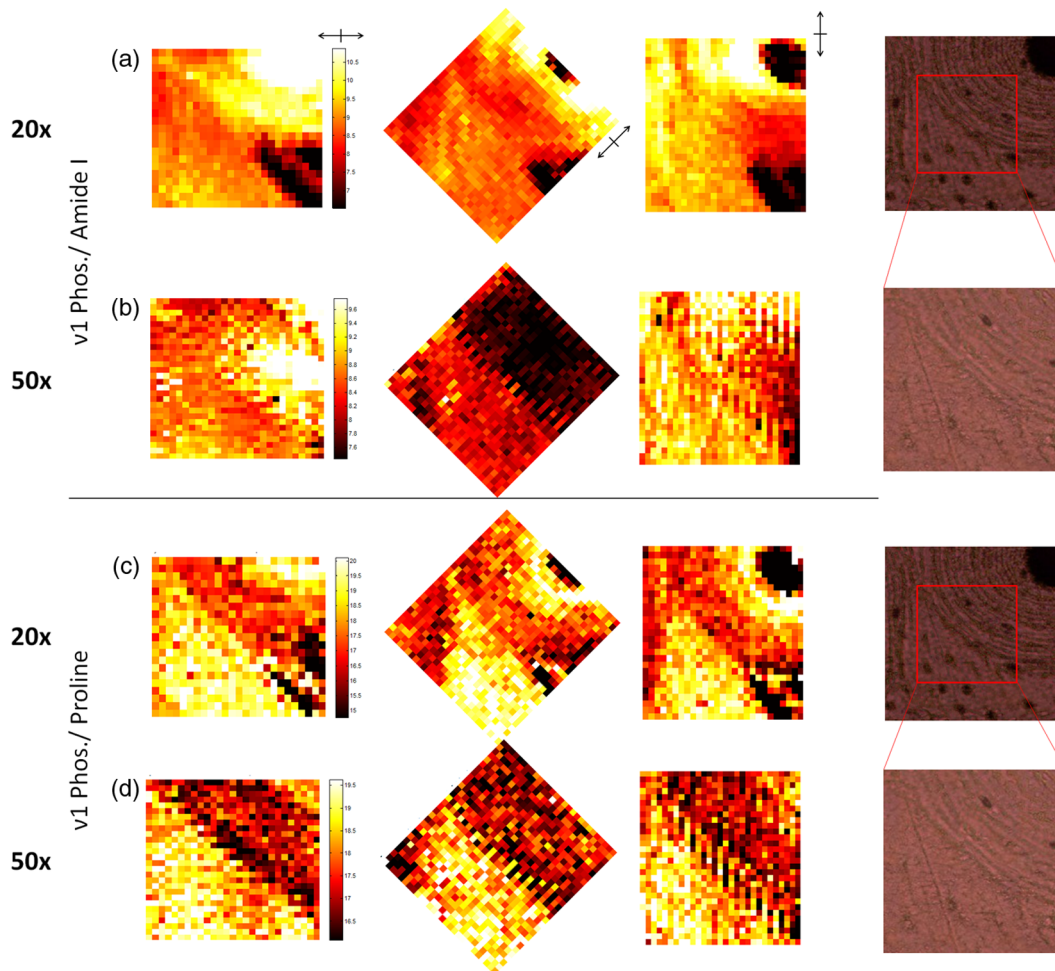


Fig. 7 Heat maps of derived peak ratios retain polarization sensitivity when rotated, even with reduction of objective numerical aperture (NA). Bright field images reference the scanned areas at 20x (NA = 0.4) and 50x (NA = 0.75). Color maps are set to universal scale within each quantity. (a) ν_1 Phosphate/Amide I maps at 20x show mild intensity changes under rotation at the border between osteonal and interstitial tissue. (b) The effect on ν_1 Phosphate/Amide I increases with increased NA in the 50x maps. (c) ν_1 Phosphate/Proline shows no notable intensity changes with rotation at 20x. (d) ν_1 Phosphate/Proline shows no notable intensity changes with rotation at 50x, but noise is increased.

predominantly organizational phenotype. Interpretation of results from these and future studies in light of instrument polarization may help to define consistent Raman signatures for compositional and organizational disease.

5 Conclusions

Polarization-orientation information in bone biomarkers, as seen in highly polarized studies involving RS, persists in unaltered commercial systems with lower inherent sensitivity to polarization. Modeling this consistent bias shows that matched phase information between peaks yields biomarker ratios that are less sensitive to polarization-orientation, without the loss of throughput necessitated by additional optics. Bias in compositional measures can be minimized by phase matching; specifically, findings support using ν_1 Phosphate/Proline for mineral to collagen and Carbonate/ ν_1 Phosphate for carbonate substitution. In the diagnosis of organizational phenotypes, polarization-orientation can be maximized by phase mismatch (i.e., ν_1 Phosphate/Amide I) without necessarily including polarization optics. Optimizing polarization in the instrument and in biomarkers should help to increase discrimination and consistency in future studies of bone.

Acknowledgments

This material is based upon work supported by the Department of Veterans Affairs, Veterans Health Administration, Office of Research and Development, Biomedical Laboratory Research and Development. The authors would also like to acknowledge financial support from NSF Grant 1068988.

References

1. S. Amin et al., "Association of hip strength estimates by finite-element analysis with fractures in women and men," *J. Bone Miner. Res.* **26**(7), 1593–1600 (2011).
2. J. A. Kanis et al., "FRAX(®) with and without bone mineral density," *Calcif. Tissue Int.* **90**(1), 1–13 (2012).
3. P. Matousek et al., "Subsurface probing in diffusely scattering media using spatially offset Raman spectroscopy," *Appl. Spectrosc.* **59**(4), 393–400 (2005).
4. M. D. Morris and G. S. Mandair, "Raman assessment of bone quality," *Clin. Orthop. Relat. Res.* **469**(8), 2160–2169 (2011).
5. M. V. Schulmerich et al., "Noninvasive Raman tomographic imaging of canine bone tissue," *J. Biomed. Opt.* **13**(2), 020506 (2008).
6. M. V. Schulmerich et al., "Transcutaneous Raman spectroscopy of murine bone *in vivo*," *Appl. Spectrosc.* **63**(3), 286–295 (2009).

7. M. V. Schulmerich et al., "Transcutaneous fiber optic Raman spectroscopy of bone using annular illumination and a circular array of collection fibers," *J. Biomed. Opt.* **11**(6), 060502 (2006).
8. B. R. McCreadie et al., "Bone tissue compositional differences in women with and without osteoporotic fracture," *Bone* **39**(6), 1190–1195 (2006).
9. A. Awonusi, M. D. Morris, and M. M. Tecklenburg, "Carbonate assignment and calibration in the Raman spectrum of apatite," *Calcif. Tissue Int.* **81**(1), 46–52 (2007).
10. J. S. Yerramshetty and O. Akkus, "The associations between mineral crystallinity and the mechanical properties of human cortical bone," *Bone* **42**(3), 476–482 (2008).
11. J. S. Yerramshetty, C. Lind, and O. Akkus, "The compositional and physicochemical homogeneity of male femoral cortex increases after the sixth decade," *Bone* **39**(6), 1236–1243 (2006).
12. J. A. Timlin et al., "Raman spectroscopic imaging markers for fatigue-related microdamage in bovine bone," *Anal. Chem.* **72**(10), 2229–2236 (2000).
13. J. G. Ramasamy and O. Akkus, "Local variations in the micromechanical properties of mouse femur: the involvement of collagen fiber orientation and mineralization," *J. Biomech.* **40**(4), 910–918 (2007).
14. O. Akkus, F. Adar, and M. B. Schaffler, "Age-related changes in physicochemical properties of mineral crystals are related to impaired mechanical function of cortical bone," *Bone* **34**(3), 443–453 (2004).
15. E. R. Draper et al., "Novel assessment of bone using time-resolved transcutaneous Raman spectroscopy," *J. Bone Miner. Res.* **20**(11), 1968–1972 (2005).
16. P. Matousek et al., "Noninvasive Raman spectroscopy of human tissue *in vivo*," *Appl. Spectrosc.* **60**(7), 758–763 (2006).
17. C. A. Patil et al., "Integrated system for combined Raman spectroscopy-spectral domain optical coherence tomography," *J. Biomed. Opt.* **16**(1), 011007 (2011).
18. J. S. Nyman et al., "Measuring differences in compositional properties of bone tissue by confocal Raman spectroscopy," *Calcif. Tissue Int.* **89**(2), 111–122 (2011).
19. S. Gamsjaeger et al., "Cortical bone composition and orientation as a function of animal and tissue age in mice by Raman spectroscopy," *Bone* **47**(2), 392–399 (2010).
20. C. B. Juang, L. Finzi, and C. J. Bustamante, "Design and application of a computer-controlled confocal scanning differential polarization microscope," *Rev. Sci. Instrum.* **59**(11), 2399–2408 (1988).
21. S. Gourion-Arsiquaud et al., "Use of FTIR spectroscopic imaging to identify parameters associated with fragility fracture," *J. Bone Miner. Res.* **24**(9), 1565–1571 (2009).
22. S. J. Gadaleta et al., "Fourier transform infrared microscopy of calcified turkey leg tendon," *Calcif. Tissue Int.* **58**(1), 17–23 (1996).
23. S. J. Gadaleta et al., "Polarized FT-IR microscopy of calcified turkey leg tendon," *Connect. Tissue Res.* **34**(3), 203–211 (1996).
24. M. E. Szabo et al., "Similar damage initiation but different failure behavior in trabecular and cortical bone tissue," *J. Mech. Behav. Biomed. Mater.* **4**(8), 1787–1796 (2011).
25. J. S. Nyman et al., "Differential effects between the loss of MMP-2 and MMP-9 on structural and tissue-level properties of bone," *J. Bone Miner. Res.* **26**(6), 1252–1260 (2011).
26. J. R. Maher et al., "Raman spectroscopy detects deterioration in biomechanical properties of bone in a glucocorticoid-treated mouse model of rheumatoid arthritis," *J. Biomed. Opt.* **16**(8), 087012 (2011).
27. B. Z. Gevorkian, N. E. Arnotskaia, and E. N. Fedorova, "Study of bone tissue structure using polarized Raman spectra," *Biofizika* **29**(6), 1046–1052 (1984).
28. M. Kazanci et al., "Bone osteonal tissues by Raman spectral mapping: orientation-composition," *J. Struct. Biol.* **156**(3), 489–496 (2006).
29. G. Falgayrac et al., "New method for Raman investigation of the orientation of collagen fibrils and crystallites in the Haversian system of bone," *Appl. Spectrosc.* **64**(7), 775–780 (2010).
30. M. Raghavan et al., "Quantitative polarized Raman spectroscopy in highly turbid bone tissue," *J. Biomed. Opt.* **15**(3), 037001 (2010).
31. D. A. Long, "Intensities in Raman spectra. I. A bond polarizability theory," *Proc. R. Soc. Lond. A Mat.* **217**(1129), 203–221 (1953).
32. G. Placzek, "Rayleigh-streuung und Raman-effekt," in *Handbuch der Radiologie*, E. Marx, Ed., pp. 205–374, Akademische Verlagsgesellschaft, Leipzig, Germany (1934).
33. A. Bonifacio and V. Sergio, "Effects of sample orientation in Raman microspectroscopy of collagen fibers and their impact on the interpretation of the amide III band," *Vib. Spec.* **53**(2), 314–317 (2010).
34. G. Leroy et al., "Human tooth enamel: a Raman polarized approach," *Appl. Spectrosc.* **56**(8), 1030–1034 (2002).
35. A. C. T. Ko et al., "Detection of early dental caries using polarized Raman spectroscopy," *Opt. Express* **14**(1), 203–215 (2006).
36. A. Masic et al., "Observations of multiscale, stress-induced changes of collagen orientation in tendon by polarized Raman spectroscopy," *Biomacromolecules* **12**(11), 3989–3996 (2011).
37. M. Kazanci et al., "Raman imaging of two orthogonal planes within cortical bone," *Bone* **41**(3), 456–461 (2007).
38. M. Kozielski et al., "Determination of composition and structure of spongy bone tissue in human head of femur by Raman spectral mapping," *J. Mater. Sci. Mater. Med.* **22**(7), 1653–1661 (2011).
39. C. A. Lieber and A. Mahadevan-Jansen, "Automated method for subtraction of fluorescence from biological Raman spectra," *Appl. Spectrosc.* **57**(11), 1363–1367 (2003).
40. A. Robichaux-Viehoever et al., "Characterization of Raman spectra measured *in vivo* for the detection of cervical dysplasia," *Appl. Spectrosc.* **61**(9), 986–993 (2007).
41. S. Porto, J. Giordmaine, and T. Damen, "Depolarization of Raman scattering in calcite," *Phys. Rev.* **147**(2), 608–611 (1966).
42. M. D. Levenson, "Polarization techniques in coherent Raman spectroscopy," *J. Raman. Spectrosc.* **10**(1), 9–23 (1981).
43. E. Hecht and A. Zajac, *Optics*, Addison-Wesley Pub. Co., Reading, Massachusetts (1987).
44. E. Malus, "Mémoires de physique et de chimie de la Société d'Arcueil," (1809).
45. J. A. Nelder and R. Mead, "A simplex method for function minimization," *Comput. J.* **7**(4), 308–313 (1965).
46. A. Ascenzi and E. Bonucci, "The tensile properties of single osteons," *Anat. Rec.* **158**(4), 375–386 (1967).
47. M. G. Ascenzi and A. Lomovtsev, "Collagen orientation patterns in human secondary osteons, quantified in the radial direction by confocal microscopy," *J. Struct. Biol.* **153**(1), 14–30 (2006).
48. R. B. Martin and D. L. Boardman, "The effects of collagen fiber orientation, porosity, density, and mineralization on bovine cortical bone bending properties," *J. Biomech.* **26**(9), 1047–1054 (1993).
49. R. B. Martin and J. Ishida, "The relative effects of collagen fiber orientation, porosity, density, and mineralization on bone strength," *J. Biomech.* **22**(5), 419–426 (1989).
50. R. B. Martin et al., "Collagen fiber organization is related to mechanical properties and remodeling in equine bone. A comparison of two methods," *J. Biomech.* **29**(12), 1515–1521 (1996).
51. W. Wagermaier et al., "Spiral twisting of fiber orientation inside bone lamellae," *Biointerphases* **1**(1), 1–5 (2006).
52. X. Bi et al., "Raman and mechanical properties correlate at whole bone- and tissue-levels in a genetic mouse model," *J. Biomech.* **44**(2), 297–303 (2011).
53. T. Buchwald et al., "Identifying compositional and structural changes in spongy and subchondral bone from the hip joints of patients with osteoarthritis using Raman spectroscopy," *J. Biomed. Opt.* **17**(1), 017007 (2012).